Optics and Lasers in Engineering 51 (2013) 278–285

Contents lists available at SciVerse ScienceDirect

Optics and Lasers in Engineering

journal homepage: www.elsevier.com/locate/optlaseng

Stereo-Digital Image Correlation (DIC) measurements with a single camera using a biprism

K. Genovese [a,*], L. Casaletto [a], J.A. Rayas [b], V. Flores [b], Amalia Martinez [b]

[a] Dipartimento di Ingegneria e Fisica dell'Ambiente, Università degli Studi della Basilicata, Potenza, Italy
[b] Centro de Investigaciones en Óptica, León, Gto., Mexico

ARTICLE INFO

Article history:
Received 6 June 2012
Received in revised form
3 October 2012
Accepted 4 October 2012
Available online 30 October 2012

Keywords:
Pseudo-stereo system
Biprism
Digital image correlation
3D deformation measurement

ABSTRACT

In this paper we present and test a Digital Image Correlation (DIC)-based single camera pseudo-stereo system that uses a biprism in front of the camera objective to split the scene into two equivalent lateral stereo views in the two halves of the sensor. Such optical arrangement simplifies image pairs matching and, more importantly, makes possible a compact set-up suitable for miniaturization. To correct the image distortion caused by the refraction through the biprism, a proper optimization-based procedure is used to map the 3D reconstruction error function over the entire measurement volume. The inverse of the volumetric distortion function is then applied to the double-image of a spherical sample placed in an arbitrary position to evaluate the shape reconstruction accuracy. Finally, the capability of the proposed system to accurately track deformation in real-time is tested via an inflation test on a circular latex membrane.

1. Introduction

Stereo Digital Image Correlation (Stereo-DIC) is a well-assessed non-contact optical technique capable of performing shape and 3D deformation measurements on length scales ranging from microns to meters with a time resolution up to nanoseconds [1–7]. A series of image pairs captured from two different views of the object are used to locate and track a given set of surface points during motion and/or deformation. To correlate the two stereo-views, DIC requires the object surface to be provided with a random pattern of dark and light features. This allows finding the best match between corresponding points in the two images by comparing the local grey scale distribution of square pixel subsets on the basis of the normalized cross correlation coefficient [1]. An efficient matching operation requires the two images to be similar in terms of speckle pattern appearance. This can be achieved by using a pair of 'twin' cameras (with identical settings) and proper illumination, or by capturing both views simultaneously with one single camera and additional external optical devices. The latter option strongly facilitates correspondence-searching reliability and further eliminates the need for hardware and software synchronization entailed in time-resolved measurements.

Several designs of compact pseudo-stereo systems using one single camera have been proposed in literature. Two virtual stereo-views of the same object can be captured by a single camera by using two differently angled planar mirrors, a glass plate at two different rotational positions, two fixed mirrors and a third rotating mirror, ellipsoidal, hyperboloidal and paraboloidal mirrors, etc. (see e.g. [8] and references therein for an extensive review of some representative single-camera stereo systems along with their performances and limitations).

In this paper we present a single-camera stereo system that uses a biprism in front of the objective to split the image in two sub-images corresponding to two virtual lateral stereo-views in the two halves of the sensor. Similar basic designs for binocular and trinocular stereovision systems using prisms have been already proposed in the computer vision literature [9,10]. However, these systems present two main limitations: (i) image formation scheme is formulated on the basis of simplifying assumptions on the relative position and orientation between camera and prism, and (ii) the significant amount of image distortion introduced by the prism is ignored.

Our work aimed to overcome these two limitations by developing and testing a biprism-single camera (BSC) system suitable for highly accurate time-resolved deformation measurement via DIC. In particular, we adopted a robust generalized stereo-system calibration framework that is insensitive to camera/biprism misalignments and we implemented a model-free optimization-based procedure to map and correct the image distortion error introduced by the biprism over the entire measurement volume.

* Corresponding author. Tel.: +39 320 4371285; fax: +39 0971 205160.
E-mail addresses: katia.genovese@unibas.it, katia.genovese@libero.it (K. Genovese).

0143-8166/$ - see front matter © 2012 Elsevier Ltd. All rights reserved.
http://dx.doi.org/10.1016/j.optlaseng.2012.10.001

A large variety of model-based approaches have been proposed in literature to deal with image distortion removal when using optical systems with low-cost video optics or wide-angle and fish-eye lenses [11–15]. Using a lens distortion model implies the definition of a *global* rule to correct the entire image. Most commonly the distortion is modeled as a parametric non-linear polynomial function of the distance ρ of the generic point of the image to the distortion center. The typical formula combines the three major components of lens distortion: the radial, the decentering and the thin prism distortions [12]. The distortion parameters can be estimated along with the intrinsic and extrinsic parameters of the camera model via non-linear optimization schemes, or, alternatively, they can be calculated after the camera has been calibrated according to an idealized pin-hole model (see [16] for a more detailed survey and a quantitative comparison performances of the most frequently used calibration and model-based distortion correction techniques).

More recently, model-free approaches based on *local* correction of the distortion have been presented in literature in an attempt to improve the performances of existing model-based methods [17] or for dealing more accurately with complex imaging systems such as stereo optical microscopes [18] and scanning electron microscopes [19,20]. In fact, although the classical parametric model-based methods have been demonstrated to be a sophisticated approach for common digital cameras and off-the-shelf objectives, they appear to be inadequate when strong local gradients of distortion are present [1,18–20].

In this work, a visual inspection of the original and after-distortion-correction images revealed that the biprism induces a distortion pattern which does not corresponding to any of the pre-defined parametric functions commonly used for correcting lens distortion. Hence, we chose to implement a model-free approach by calculating a 'piece-wise' function describing the local character of the image deformation over the entire measurement volume. To this end, a 3D set of fiducial points was generated through multiple acquisitions of a planar target sequentially positioned in order to 'scan' the entire volume of interest. In this way, along with the distortion induced by the biprism, other kinds of distortion effects depending on the depth (e.g. in the case of high-magnification view, as will be the case for the future development of a hand-held 3D optical probe for the examination of skin lesions) are automatically included and corrected.

2. Materials and methods

2.1. Experimental set-up

Fig. 1 schematically illustrates the rationale behind the proposed pseudo stereo-system. When a biprism is placed in front of a single CCD camera, two different views of the object behind the biprism are simultaneously imaged on the two halves of the sensor (Fig. 2). In an ideal perfectly aligned system, by performing a simple ray-tracing procedure, it is possible to find the exact position and orientation of the two virtual stereo-cameras as a function of the characteristics of the biprism (index of refraction n_p, angle α, thickness s) and of the relative distances of object-biprism (d_O) and camera-biprism (d_C) [9]. The stereo-angle of the virtual-stereo system is directly related to α, while the lateral separation between the two sub-images on the two halves of the sensor depends on s, d_O and d_C. In this work, the theoretical formulation of the image formation [9] was used only during the preliminary stage of the system design to find the geometry of the biprism best suited for the camera characteristics and the dimension of the sample of interest. Indeed, one of the objectives of this work was to establish a calibration procedure that does not rely on prior knowledge of any of the above mentioned parameters to find the position and orientation of the two virtual cameras of the BSC system.

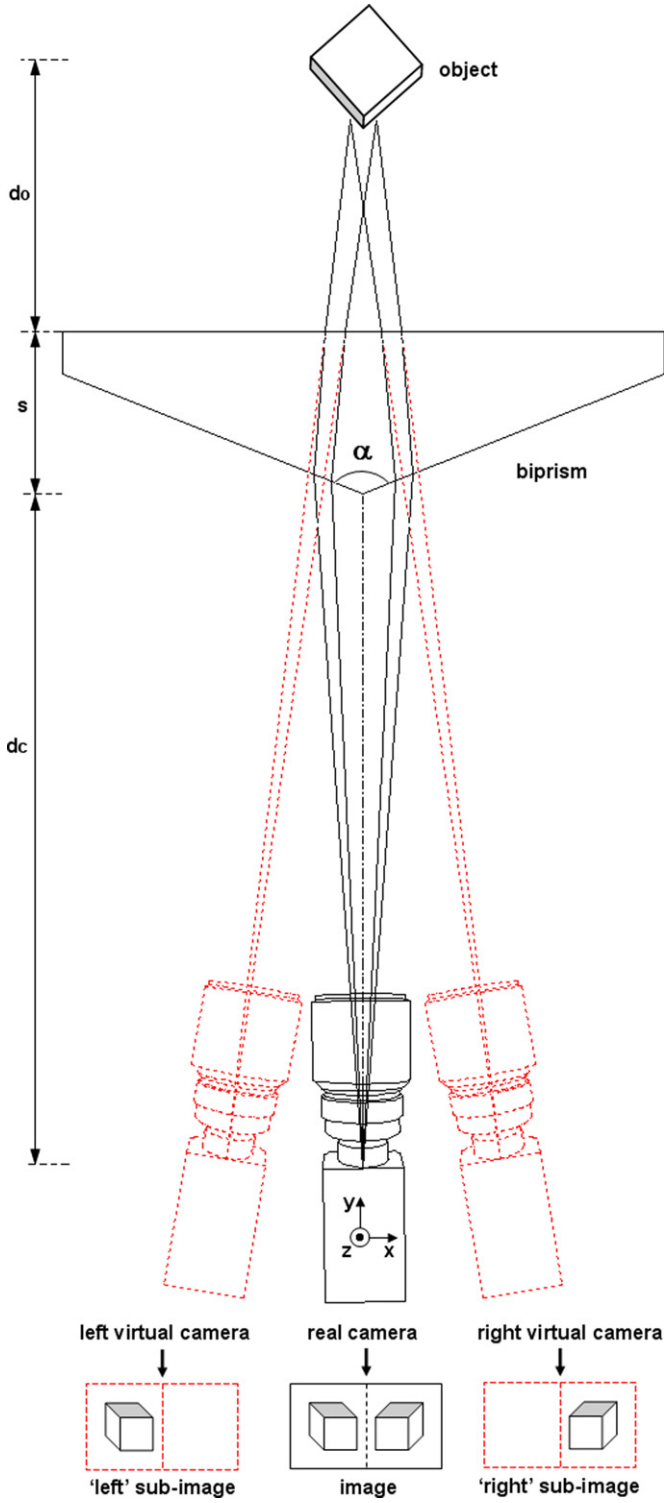

Fig. 1. Image formation scheme for the biprism-single camera (BSC) pseudo-stereo system.

Fig. 3 shows a picture of the final experimental set-up. A biprism (n_p=1.4585, α=161.4°, s=30 mm, surface quality=40/60, surface accuracy=λ/4, Centro de Investigaciones en Óptica,

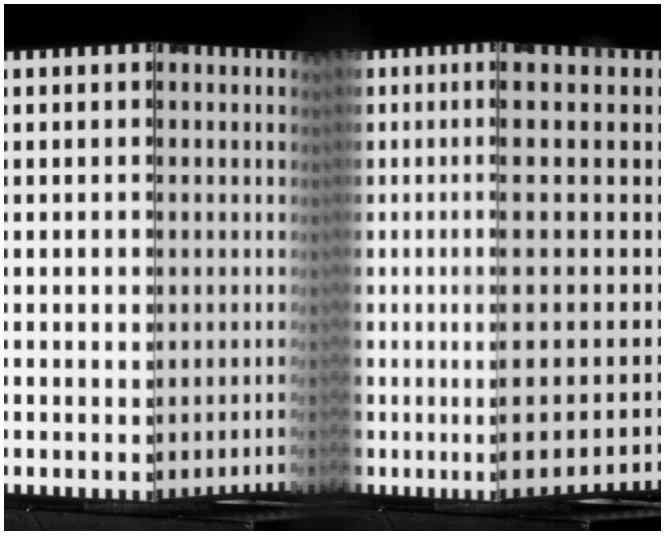

Fig. 2. A cube target with a regular dot pattern as seen by the BSC system.

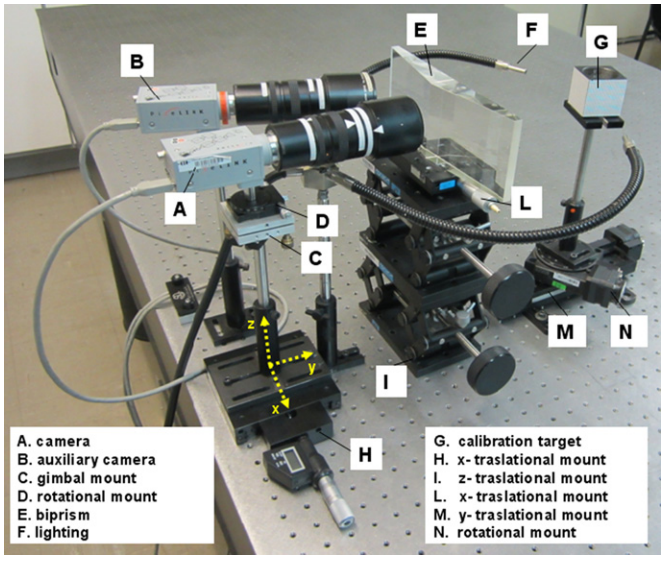

Fig. 3. Picture of the experimental set-up.

León, Gto., MX) is fixed on the top of two lab jacks stacked in order to allow vertical adjustment through a total distance of 84 mm. A 1280×1024 8-bit B/W CCD camera equipped with a zoom 7000 macro NAVITAR objective (focal length 18–108 mm, F-stop 2.5-28C) is placed onto a series of mounts that allows the camera to be translated, rotated and tilted for fine adjustment with respect to the biprism. The object (in Fig. 3 a cube target with a regular square dots pattern on two adjacent faces) is placed onto a motorized rotational mount (range=360°, resolution=0.01°) fixed to a motorized long travel translation mount (travel range=100 mm, resolution=2.5 μm). Lighting is provided by a dual gooseneck fiber optic illuminator equipped with a red filter (centered on $\lambda=630$ nm, bandwidth $\Delta\lambda=20$ nm) to reduce the chromatic aberration introduced by the biprism. An auxiliary twin-camera is placed at an angle of about 20° with respect to the primary camera. This served to provide a standard lateral stereo-system used as reference for set-up and evaluation of the relative merits of the BSC system.

2.2. BSC system alignment and calibration

The first step of the experimental procedure consisted of aligning the primary camera with the biprism. First, the two cameras were set on identical parameters, positioned at the same height and pointed at the object from two angled views. Then, the biprism was positioned in order to be fairly centered to the lens objective of the primary camera. Finally, by operating the multi-axial mounts, both the primary camera and the biprism were finely adjusted such that the front edge of the biprism split the camera field of view in two halves and the back face of the biprism and camera sensor were reasonably parallel (according to the layout in Fig. 1). Since the system calibration procedure proposed here is not based on the knowledge on the mutual position and orientation of camera and biprism, this preliminary alignment is not strictly required although it is recommended for obtaining evenly symmetric sub-images thus improving the overall accuracy of the measurement.

The second step of the experimental procedure consisted in calibrating the BSC system. In computer-vision-based measurement, camera calibration allows the 3D information to be inferred from the 2D information coded into the images. The camera model here considered is the pin-hole model, i.e. the camera is assumed to perform a perfect perspective transformation. As a matter of fact, the images are affected by a serious distortion caused by the nonlinear angle variation and to the varying optical path of the non-collimated light rays through the biprism. Hence, a post-calibration procedure is needed to find the transformation (i.e. the un-distortion function) that maps the actual images onto a distortion-free image data set following the perspective camera model.

The calibration/distortion correction procedure was performed through the steps described below.

2.2.1. Standard stereo-system calibration and reference points data reconstruction

The biprism was lowered by adjusting on the lab jacks in order to clear the field of view of the two cameras. The corner of a cube with a regular square dots pattern on it (pitch=2 mm, labeled with G in Fig. 3) was imaged from the standard stereo-system in a position along the y axis, hereafter referred to as POS.0. This served to calibrate the two cameras by using the Direct Linear Transformation (DLT) method described in detail in [21]. Briefly, the DLT method uses a set of control points whose 3D coordinates in a arbitrary global reference system are known with high accuracy (i.e. the dot calibration pattern on the two faces of the cube) to find a set of 11 coefficients that are functions of the intrinsic and extrinsic parameters of each camera. In particular, these coefficients are the unknowns of the overdetermined system built on mapping each 3D control point world coordinates (x,y,z) into its corresponding 2D image coordinates (η,ξ) through a perfect perspective transformation as follows:

$$(\eta-\eta_0)=l\cdot s_\eta\frac{(M_{xx}x+M_{xy}y+M_{xz}z+\delta_x)}{(M_{zx}x+M_{zy}y+M_{zz}z+\delta_z)}$$
$$(\xi-\xi_0)=l\cdot s_\xi\frac{(M_{yx}x+M_{yy}+M_{yz}z+\delta_y)}{(M_{zx}x+M_{zy}y+M_{zz}z+\delta_z)} \quad (1)$$

where l (mm)(focal length), η_0,ξ_0 (pixel) (coordinates of the center C of the sensor) and s_η,s_ξ (pixel/mm) (scale factors) are the intrinsic parameters of the camera, while M_{rs} (r, s=x, y, z) (components of the rotation matrix) and δ_r (mm) (components of the translation vector) are the extrinsic parameters i.e. they define position and orientation of the camera with respect to the global reference system. By introducing the DLT parameters $L_i(i=1,\ldots,11)$ that are functions of the unknown intrinsic and

extrinsic parameters of each camera system, Eq. (1) can be rearranged as:

$$\eta = \frac{L_1x+L_2y+L_3z+L_4}{L_9x+L_{10}y+L_{11}z+1}$$

$$\xi = \frac{L_5x+L_6y+L_7z+L_8}{L_9x+L_{10}y+L_{11}z+1} \quad (2)$$

Each control point provides two equations, thus a minimum of $n=6$ control points are needed to extract the entire set of DLT parameters and hence to calibrate each camera. Usually, n is chosen to be much larger than six in order to get an over-determined system and thus to reduce the effect of experimental errors through a linear least-squares based approach.

Once the two cameras were calibrated, the standard stereo-system was used to retrieve the 3D position of a new set of more than 3000 points evenly distributed over a volume of $18\times46\times34$ mm^3 (width × height × depth, along the x, z and y direction of Fig. 3, respectively). This 3D control points grid was obtained by first rotating the cube target about the z axis to orient one face parallel to the primary camera sensor. Then, the target was translated through 17 evenly spaced increments of 2 mm around POS.0 (POS.−8, POS.−7,…, POS.+7 and POS.+8 hereafter); for each position, the 3D coordinates of a set of 23×9 control points on the target face was reconstructed via the previously calibrated stereo-system. A LabVIEW code allowed for automatic rotation and translation of the target by means of the two high-precision motorized mounts (labeled with N and M, respectively, Fig. 3, maximum error of repeatability in repositioning$=\lambda/10$ evaluated via interferometry) and for automatic capture of images at each configuration of interest.

Although the retrieved position is not the 'error-free' position of the volumetric point cloud (due to the reconstruction error d of the standard Stereo-DIC measurement $d=0.021$ mm $\pm$ 0.032 mm calculated as the Eucledian distance between reconstructed and theoretical point positions), it served to build a volume of $m=207\times17$ evenly spaced control points (207 dots over the target face—xz plane—and 17 positions of the target along the depth—y axis-) to be used as a reference in the subsequent phase of retrieval of the volumetric distortion function.

2.2.2. Evaluation of the volumetric distortion function

The biprism was raised back by adjusting the lab jacks in order to fill the field of view of the primary camera. A series of configurations identical to step-1 were considered but, this time, for each target position, a single image was captured from the primary camera through the biprism. Each image contained two sub-images (see Figs. 1 and 2) that were virtually equivalent to the two views of a lateral stereo-system. Analogously to step-1, the collected images were processed first by calibrating the virtual stereo system (with the cube target in POS.0), and then reconstructing the control grid of one single face sequentially moved through POS.−8 to POS.+8. As expected, the images captured with the BSC system present an evident distortion (visible with naked eye, see Fig. 2). Hence, when these images are processed by using an idealized pin-hole projection scheme, the 3D reconstruction is affected by a significant error. As an example, Fig. 4a shows the reconstruction error (calculated as the Euclidean distance d between reconstructed points and corresponding theoretical points) for the calibration target in POS.0.

In this work we implemented a post-calibration procedure that first maps the 3D distribution of the reconstruction error and later corrects it on the basis of a local approach. In particular, the proposed methodology results in a data error reduction by evaluating the displacement induced by the distortion for each control marker in the image through an optimization-based approach (see scheme in Fig. 5). The optimization problem is formulated into the Matlab environment, by using the function *fmincon*, as follows:

- the reference position of the jk-th point out of the m volumetric cloud in the global coordinate system (retrieved with the procedure described in Section 2.2.1) is $P^T_{jk}=(x^T_{jk}, y^T_{jk}, z^T_{jk})$ (mm, mm, mm) (with $j=1,...,207$ and $k=1,...,17$);
- the erroneous position of the m control points calculated from the uncorrected BSC system images on the basis of a perfect perspective transformation is $P^{DIST}_{jk}=(x^{DIST}_{jk},y^{DIST}_{jk}, z^{DIST}_{jk})$ (mm, mm, mm) (see Fig. 5.4);
- the image of the j-th control marker on the calibration target face in the POS.k has coordinates $I^{DIST}_{R\_jk}=(\eta^{DIST}_{R\_jk},\xi^{DIST}_{R\_jk})$ (pixel, pixel) in the k-th virtual right image of the BSC system.

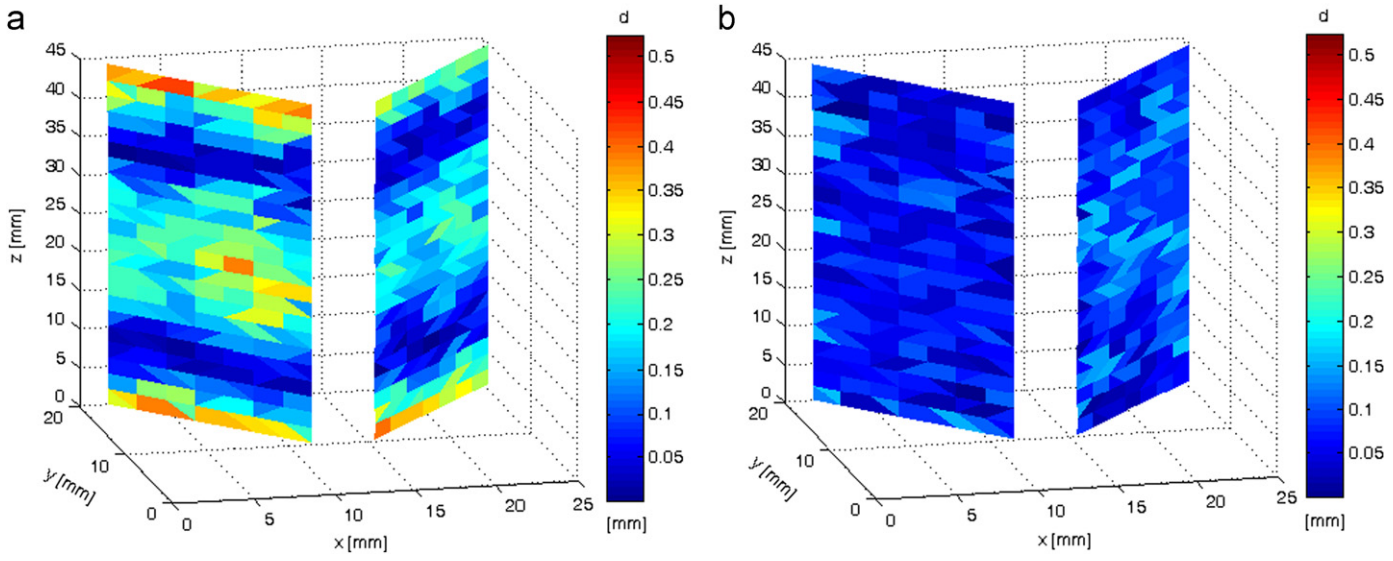

Fig. 4. Plot of the error d between theoretical 3D position of calibration points in Fig. 2 and its experimental counterpart measured with the BSC system before (a) and after distortion correction (b).

Analogously, the position of the image of the j-th control marker in the k-th virtual left image is $I^{DIST}_{L\_jk}=(\eta^{DIST}_{L\_jk},\xi^{DIST}_{L\_jk})$ (pixel, pixel);

- the unknown positions of the j-th control marker in the distortion-free k-th right and left images are $I^{CORR}_{R\_jk}=(\eta^{CORR}_{R\_jk},\xi^{CORR}_{R\_jk})$ and $I^{CORR}_{L\_jk}=(\eta^{CORR}_{L\_jk},\xi^{CORR}_{L\_jk})$, respectively;
- the distortion due to the biprism introduces a displacement u_{R/L_jk}(pixel) and v_{R/L_jk} (pixel) between I^{DIST}_{R/L_jk} and I^{CORR}_{R/L_jk} along the η and ξ directions, respectively (see Fig. 5.5);
- at each iteration, given u_{R/L_jk} and v_{R/L_jk} as variables of the optimization, the corrected position of the jk-th control marker in the virtual right image is hence defined as:

$$\eta^{CORR}_{R\_jk}=\eta^{DIST}_{R\_jk}+u_{R\_jk}\ \text{(pixel)}$$
$$\xi^{CORR}_{R\_jk}=\xi^{DIST}_{R\_jk}+v_{R\_jk}\ \text{(pixel)} \quad (3)$$

and similarly for the virtual left image.

- the objective function to be minimized is the Euclidean distance d between P^{T}_{jk} and P^{CORR}_{jk} where the 3D coordinates of P^{CORR}_{jk} are calculated at each iteration from $I^{CORR}_{R\_jk}=(\eta^{CORR}_{R\_jk},\xi^{CORR}_{R\_jk})$ and $I^{CORR}_{L\_jk}=(\eta^{CORR}_{L\_jk},\xi^{CORR}_{L\_jk})$, through a perfect perspective transformation scheme.

The non-linear optimization procedure yields four volumetric maps of error: u_R, v_R, u_L and v_L. For each error component (e.g., for $u_R(x,y,z)$), the Matlab function *griddata3*$(x^{DIST},y^{DIST},z^{DIST},u_R,x,y,z)$ is used to fit the m non-uniformly spaced vectors $(x^{DIST}_{jk},y^{DIST}_{jk},z^{DIST}_{jk},u_{R\_jk})$ with a hypersurface and, at the same time, to interpolate the value of u_R at any point (x,y,z) of interest over the entire measurement volume with a tessellation-based linear interpolation scheme that uses the 'local' information from the nearby control points. Fig. 6 shows two of the four distortion maps obtained from the BSC calibration procedure (only a few sections of the volumetric data have been plotted for clarity of representation).

It is worthwhile to point out here that the corrected images of the virtual BSC stereo-system do *not* correspond to the images of the standard stereo-system since the two systems possess different intrinsic and extrinsic parameters.

2.2.3. Validation of the distortion correction procedure

The volumetric error maps in Fig. 6 can be practically considered as the un-distortion functions to be applied to a given object point (x,y,z) reconstructed with the BSC system within the measurement volume. For example, if these un-distortion functions are applied to the virtual right and left images of the calibration target in the POS_0 (Fig. 2) the reconstruction error drops from 0.17 ± 0.10 mm (Fig. 4a) to 0.09 ± 0.05 mm (Fig. 4b), i.e. the distortion correction procedure allows 3D measurement with an accuracy comparable to that of the standard Stereo-DIC system.

To verify that the above derived volumetric un-distortion functions are not target-dependent and that they can be effectively applied to whatever object is arbitrarily placed within the measurement volume, a portion of a ping-pong ball with a sprayed speckle pattern on it, was imaged by the BSC system (Fig. 7a) and reconstructed after matching the two virtual views via DIC [1]. Fig. 7b,c reports the deviation from the reference geometry of the sample (radius$=18.265\pm0.065$ mm, measured with a spherometer in three points) for the uncorrected and

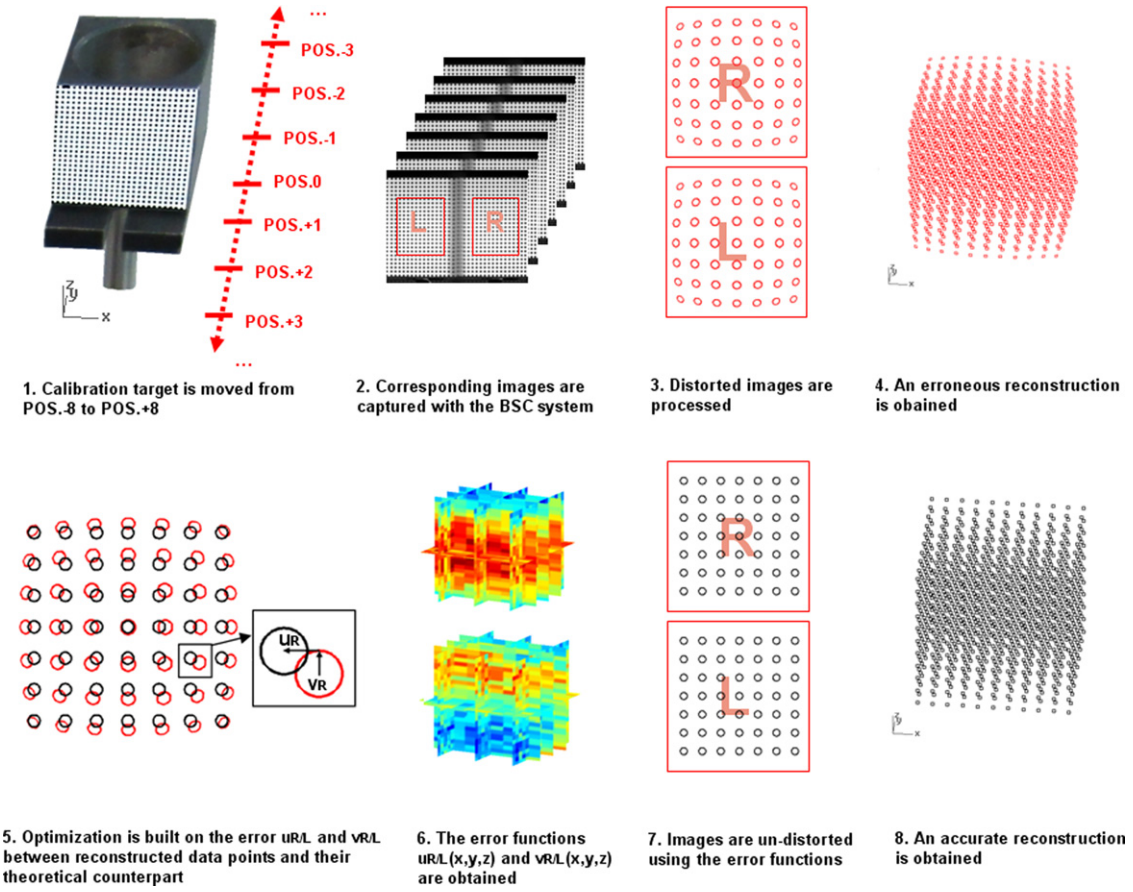

Fig. 5. Scheme of the optimization-based procedure for mapping and correcting the distortion error throughout the measurement volume.

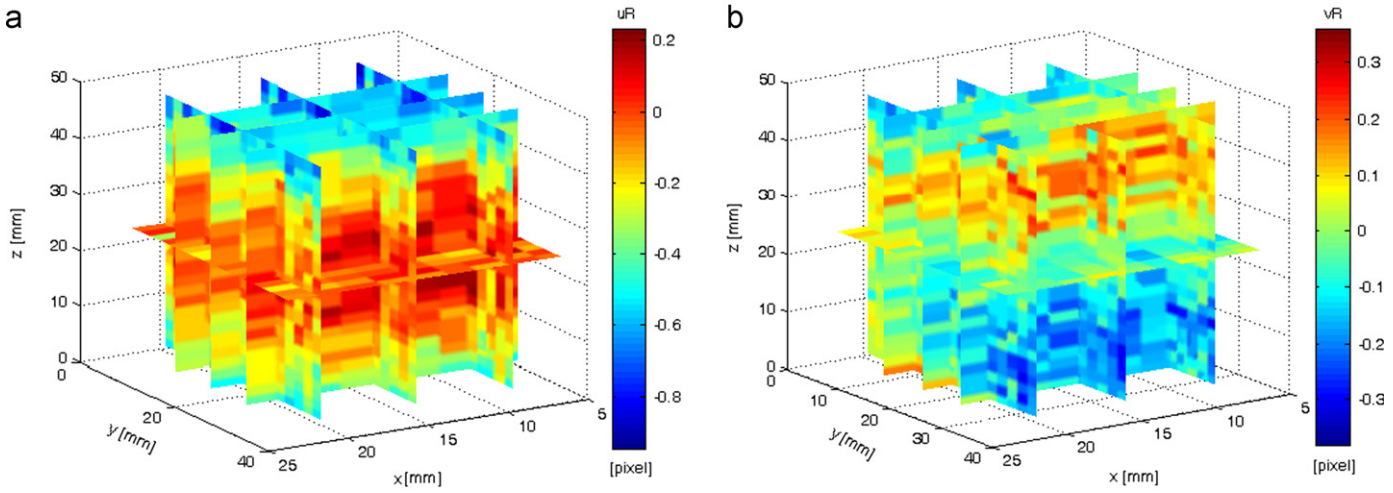

Fig. 6. 3D plot of the distributions of $u_R(x,y,z)$ and $v_R(x,y,z)$ obtained by processing the set of virtual right-hand images of the calibration pattern from POS. −8 to POS. +8. Due to the symmetry of the BSC system, the data processing for the set of virtual left-hand images yields a similar 3D distributions for $u_L(x,y,z)$ and $v_L(x,y,z)$.

corrected reconstructed shapes, respectively. Significantly, application of the un-distortion procedure reduced the error from 0.32 ± 0.10 mm (Fig. 7b) to $5.6\ 10^{-4} \pm 0.08$ mm (Fig. 7c). It is interesting to notice how the pattern of distortion in the case of the ping-pong ball is less evident than that observed for the calibration target (compare Fig. 4a with Fig. 7b). This could be explained by considering that, conversely to the case of the calibration target where the dots are located through a centroid-searching procedure, for the DIC-based measurement, control points matching was performed by employing pixel subsets of fixed dimension (in this work we used a 21×21 pixel^2 template window and a 41×41 pixel^2 analysis window, see Ref. [1] for further details on the DIC technique). This fact very likely acts as a 'smoothing' effect that mitigates the local character of the distortion without, however, affecting the effectiveness of the subsequent error correction procedure.

2.3. Inflation test on a circular latex membrane

The aim of this work was to develop and test a compact pseudo-stereo system for high accuracy full-field 3D-DIC deformation measurement. Thus, the last step of the experimental procedure consisted of using the validated BSC system for tracking via DIC the 3D deformation of a latex circular membrane under inflation. The choice of the test case was based on the fact that the proposed system was conceived as a large-scale prototype of a future miniaturized handheld optical probe to be used for biomechanical applications. In-vitro inflation (bulge) experiments are in fact a common protocol adopted for testing quasi-spherical biological parts e.g. [22,23] and biological membranes e.g. [24–26].

A piece of commercial white latex from a glove (thickness = 0.16 mm) was first sprayed with black paint by using a fine-tipped airbrush in order to provide the random speckle pattern needed for the DIC-based measurement. The membrane was then clamped with an O-ring to the circular window ($\phi = 30$ mm) of a pressurization chamber and then progressively inflated over a pressure range from 0.05 kPa to 16 kPa. During pressurization, the single camera of the BSC system recorded a frame sequence at 11 fps to be used for subsequent deformation data processing. The BSC system later allowed for extracting the shape of the inflated membrane from each single image of the sequence as well as for tracking deformation with respect to the reference configuration (at $p = 0.05$ kPa). Due to the large deformation undergone by the membrane, a serial approach was implemented to track the deformation through the sequence of images captured with the BSC system [27,28].

Fig. 8a–c shows the distortion-free 3D full-field maps of the u, v and w components of the surface displacement of the inflated latex membrane (at $p \sim 13$ kPa) along the x' z' and y' directions of a reference system centered with the undeformed circular membrane (with x' and y' axes lying in the membrane plane and z' oriented outward, see Fig. 8). In this reference system, as expected, the u and v maps show zero-displacement along the vertical and horizontal central axes respectively due to the geometry/load/constraint symmetry and to the fact that the test sample is an isotropic, homogenous membrane of constant thickness. Furthermore, the w map presents the characteristic polar-symmetrical pattern [24] with a maximum out-of-plane displacement of about 6 mm in the central region. Since only one image is needed to perform the 3D reconstruction, analogous deformation maps can be extracted from each image of the frame sequence, i.e. the time resolution of the measurement is equal to the frame acquisition rate of the video-system.

3. Discussion

In this paper, we presented and discussed a biprism/one-camera arrangement as an effective alternative to a traditional two camera stereo-system. The advantage of the proposed approach is the capability to perform 3D-DIC measurements with a single camera. This implies that the matching efficiency of stereo-pairs is optimized (since the two virtual cameras have identical settings) and that camera synchronization is not an issue for time-resolved measurements. On the other hand, the area of analysis on the test sample is greatly reduced (44% for a circle imaged into a sensor with a 3:2 aspect ratio and 70% when using a sensor with a square aspect-ratio). Decreasing the spatial resolution of an image inevitably brings a degraded resolution of the DIC-based measurement [29,30]. However, this optical arrangement has been conceived to be later miniaturized to serve for a very specific application that is the development of a handheld probe for 3D inspection in dermatology. The BSC-based optical probe will perform skin examinations on circular areas through in-vivo suction-tests (this motivated the adoption of a spherical target in par. 2.2-3 and of the inflation test in Section 2.3). Hence, given the smoothness of the geometry of interest and the large

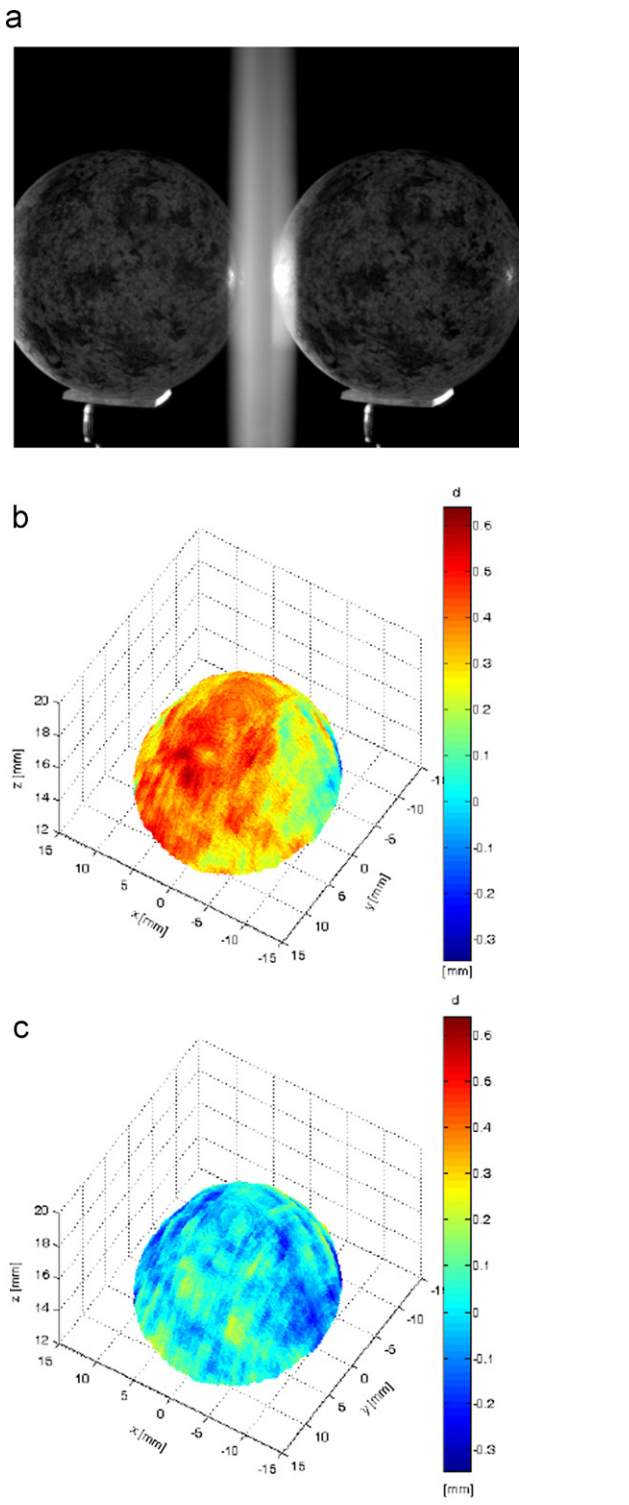

Fig. 7. 3D reconstruction of a portion of a spherical target with the DIC-BSC system: image of the sample (a), reconstruction error d (with respect to the ideal shape) before (b) and after distortion correction (c).

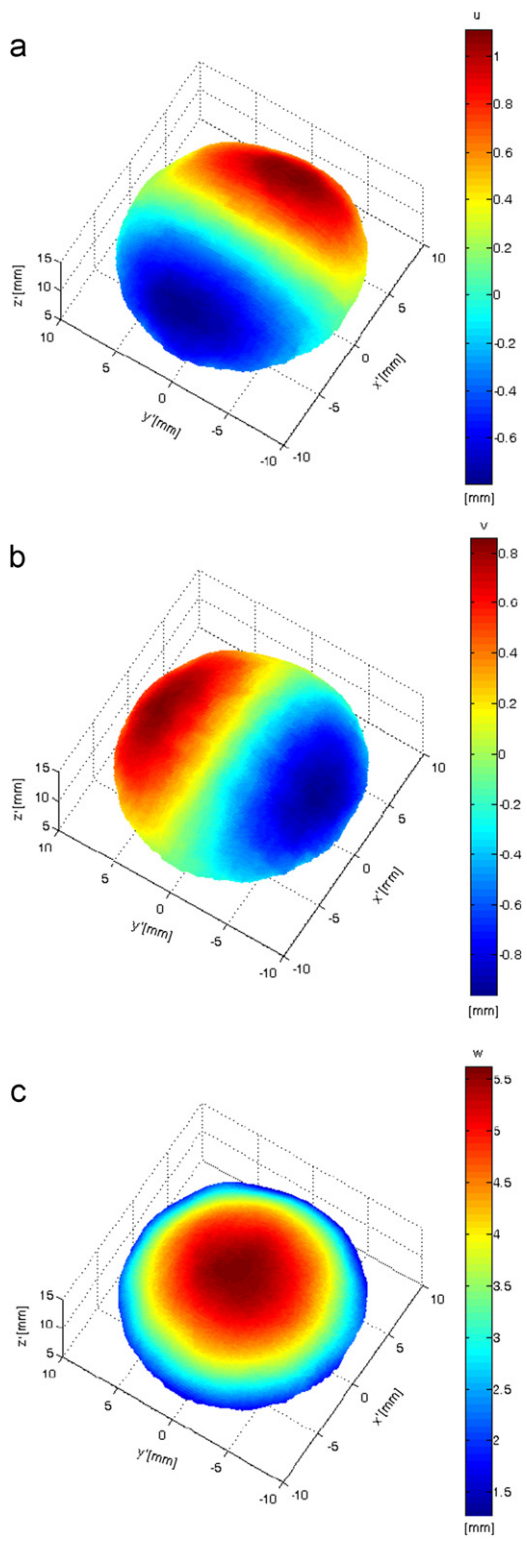

Fig. 8. 3D DIC-BSC deformation measurement on a circular latex membrane subjected to inflation: plot of the displacement components u (a), v (b) and w (c).

deformation involved in this kind of measurement, it is expected that the above mentioned loss in resolution will not significantly affect the overall quality of the measurement.

In contrast to previous similar works in the literature [9,10], the measurement procedure developed is insensitive to camera/biprism misalignment and takes into account the significant distortion introduced by the biprism. In particular, we proposed a completely generalized two-step approach for calibrating the system and mapping the reconstruction error over the entire given volumetric domain. Without assuming any pre-defined distortion model, but using an optimization-based routine and a subsequent interpolation process, all points in the measurement volume are mapped into the virtual, distortion-free counter parts that follow the perfect perspective model. The distortion correction possesses a strong local character since the error

interpolation is done in a 'piece-wise' fashion by using information only from nearby control points. This feature is expected to become of increasing importance in the presence of a high local distortion gradient as in the case of high-magnification measurements [18]. Moreover, the un-distortion function was demonstrated to be independent from the target used for calibration [17]. This implies that, once the system has been calibrated, if the relative position/orientation of camera and biprism remains unaltered (as in the case of the future BSC-based optical probe), the test sample can be placed arbitrarily within the measurement volume without affecting the measurement accuracy (a plastic spacer could serve to insure that the area of examination is within the calibrated volume).

4. Conclusion

Digital image correlation is currently the method of choice for dealing with a large variety of engineering problems since it permits acquisition of 3D-deformation information with high spatial/temporal resolution and with relatively modest investment in hardware and software requirements. In this study, we have investigated the feasibility of a compact stereo-DIC system with potential for further miniaturization and use in an optical probe for in-vivo biomechanical 3D measurements. In particular, we have designed and validated a single camera pseudo-stereo-system that uses a biprism to obtain two virtual lateral stereo-views. A model-free image distortion correction scheme demonstrated to overcome the problems related to the use of a thick prism and made it possible to perform high accuracy time-resolved 3D deformation measurements on an inflated latex membrane. The results obtained in this study are encouraging and clearly demonstrate the feasibility of the proposed approach. The capability to measure full-field 3D deformation can be particularly useful when employing inverse characterization procedures for biological membranes which may possess a considerable degree of anisotropy [24–26]. For this reason, the general feasibility of the proposed methodology for investigations in biomechanics merits further study.

Acknowledgments

This work was supported by the CONACYT-MAE Program n. 146523.

References

[1] Sutton MA, Orteu JJ, Schreier H. Image correlation for shape, motion and deformation measurements. Springer; 2009.
[2] Cárdenas-Garcia JF, Yao HG, Zheng S. 3D reconstruction of objects using stereo imaging. Opt Laser Eng 1995;22(3):193–213.
[3] Sun Z, Lyons JS, McNeill SR. Measuring microscopic deformations with digital image correlation. Opt Laser Eng 1997;27(4):409–28.
[4] Siebert T, Becker T, Spiltthof K, Neumann I, Krupka R. High-speed digital image correlation: error estimations and applications. Opt Eng 2007;46(5): 051004.
[5] Sousa AMR, Xavier J, Morais JJL, Filipe VMJ, Vaz M. Processing discontinuous displacement fields by a spatio-temporal derivative technique. Opt Laser Eng 2011;49(12):1402–12.
[6] Sozen S, Guler M. Determination of displacement distributions in bolted steel tension elements using digital image techniques. Opt Laser Eng 2011;49(12): 1428–35.
[7] Zhang R, He L. Measurement of mixed-mode stress intensity factors using digital image correlation method. Opt Laser Eng 2012;50(7):1001–7.
[8] Wang R, Li X, Zhang Y. Analysis and optimization of the stereo-system with a four-mirror adapter. J Eur Opt Soc—Rapid Publ 2008;08033:3.
[9] Lee DH, Kweon IS. A novel stereo camera system by a biprism. IEEE Trans Robotics Autom 2000;16(5):528–41.
[10] Xiao Y, Lim KB. A prism-based single-lens stereovision system: from trinocular to multi-ocular. Image Vision Comput 2007;25(11):1725–36.
[11] Brown DC. Close-range camera calibration. Photogramm Eng Remote Sens 1971;42:855–66.
[12] Weng J, Cohen P, Herniou M. Camera calibration with distortion models and accuracy evaluation. IEEE Trans Patt Anal Mach Intell 1992;14:965–80.
[13] Tsai R. A versatile camera calibration technique for high-accuracy 3D machine vision metrology using off-the-self TV camera lenses. IEEE J Robotics Autom 1997;RA-3:323–44.
[14] Zhang Z. A flexible new technique for camera calibration. IEEE Trans Pattern Anal Mach Intell 2000;22:1330–4.
[15] Devernay F, Faugeras O. Straight lines have to be straight. Mach Vis Appl 2001;13:14–24.
[16] Salvi J, Armangué X, Batle J. A comparative review of camera calibration methods with accuracy evaluation. Pattern Recognition 2002;35:1617–35.
[17] Ricolfe-Viala C, Sánchez-Salmerón A-J. Correcting non-linear lens distortion in cameras without using a model. Opt Lasers Technol 2010;42:628–39.
[18] Schreier HW, Garcia D, Sutton MA. Advances in light microscope stereo vision. Exp Mech 2004;44(3):278–88.
[19] Sutton MA, Li N, Joy DC, Reynolds AP, Li X. Scanning electron microscopy for quantitative small and large deformation measurements part I: SEM imaging at magnifications from 200 to 10,000. Exp Mech 2007;47(6):775–87.
[20] Sutton MA, Li N, Garcia D, Cornille N, Orteu JJ, McNeill SR, et al. Scanning electron microscopy for quantitative small and large deformation measurements. Part II: Experimental validation for magnifications from 200 to10,000. Exp Mech 2007;47(6):789–804.
[21] Abdel-Aziz YI, Karara HM. Direct linear transformation from comparator coordinates into object space coordinates in close range photogrammetry. Proceedings of the ASP/UI symposium on close-range photogrammetry, Urbana, Illinois, p. 1–8; 1971.
[22] David G, Pedrigi RM, Heistand MR, Humphrey JD. Regional multiaxial mechanical properties of the porcine anterior lens capsule. J Biomech Eng 2007;129(1):97–104.
[23] Boyce BL, Grazier JM, Jones RE, Nguyen TD. Full-field deformation of bovine cornea under constrained inflation conditions. Biomaterials 2008;29: 3896–904.
[24] Cosola E, Genovese K, Lamberti L, Pappalettere C. Mechanical characterization of biological membranes with moiré techniques and multi-point simulated annealing. Exp Mech 2008;48:465–78.
[25] Kim JH, Avril S, Duprey A, Favre JP. Experimental characterization of rupture in human aortic aneurysms using a full-field measurement technique. Biomech Modeling Mechanobiol 2012;11(6):841–53.
[26] Khatyr F, Imberdis C, Varchon D, Lagarde JM, Josse G. Measurement of the mechanical properties of the skin using the suction test. Skin Res Technol 2006;12-1:24–31.
[27] Zhengzong T, Jin L, Zhengzong X, Cheng G. Large deformation measurement scheme for 3D digital image correlation method. Opt Laser Eng 2012;50/2: 122–30.
[28] Bing P, Wu D, Xia Y. Incremental calculation for large deformation measurement using reliability-guided digital image correlation. Opt Laser Eng 2012;50(4):586–92.
[29] Sun Y, Pang JHL. Study of optimal subset size in digital image correlation of speckle pattern images. Opt Laser Eng 2007;45(9):967–74.
[30] Bornert M, Brémand F, Doumalin P, Dupré JC, Fazzini M, Grédiac M, et al. Assessment of digital image correlation measurement errors: methodology and results. Exp Mech 2009;49/3:353–70.